IR/RF REFRACTIVITY PROFILES OVER COASTAL WATER

Gerrit de Leeuw, Filip P. Neele and Alexander M.J. van Eijk
TNO Physics and Electronics Laboratory
P.O. Box 96864
2509 JG The Hague
The Netherlands

1. SUMMARY

In June 1992, IR/RF propagation experiments were conducted over the North Sea, at about 10 km SW from the German Island of Sylt. The experiments were a tri-lateral cooperation between institutes from Germany, Canada and The Netherlands, organized by the TNO Physics and Electronics Laboratory. The objective was a study on the complementarity of IR and radar detection systems.

In this contribution we report on the characterization of the propagation environment by the TNO Physics and Electronics Laboratory. This includes aerosol and lidar measurements to determine the extinction properties throughout the marine atmospheric boundary layer, as well as measurements of humidity and temperature profiles in the marine atmospheric surface layer to determine refractivity profiles.

Temperature and humidity profiles were measured form a jack-up barge 'Hubinsel Barbara' and on a mast. The sensors were mounted such that profiles could be measured from close to the sea surface, taking into account tidal effects and waves of 1.5 m, to heights of 10 m on the mast and 35 m on the platform. The platform data are often perturbed. Therefore, in the analysis we focussed on the temperature and humidity profiles from the mast. Effects of sensor height, wind speed and thermal stratification were considered. Deviations from the logarithmic behaviour have been observed. These are mainly ascribed to coastal influences, based on consideration of the height dependence and the effects of thermal stability. We conclude that in off-shore winds non-equilibrium situations often exist at the sensor locations, with an internal boundary layer that distorts the profiles.

2. INTRODUCTION

The performance of electro-optical systems for detection or identification of targets strongly depends on atmospheric conditions. A detailed knowledge of the effects of aerosols, temperature and humidity gradients, and turbulence on the propagation of electromagnetic radiation is important for both forecasting the propagation conditions (e.g., maximum range of detection of targets) and the interpretation of observations; range prediction is valuable as a TDA (tactical decision aid) for *a priori* assessment of the value of electro-optical detection systems. Over sea, IR detection systems are complementary to RF systems because of the differences in refraction properties as function of atmospheric structure.

When atmospheric conditions are such that electromagnetic waves are bent towards the Earth's surface, it is possible to observe targets beyond the geometrical horizon. In this case the atmospheric structure is super-refractive. Sub-refraction occurs when waves are bent away from the surface. Beaulieu[6] shows that for radar frequencies (RF) the dew-point-to-sea-temperature (DSTD) determines the refractive structure near the sea surface, super-refraction occurring for negative DSTD. For infra-red (IR) waves the air-to-sea-temperature difference (ASTD) is a useful parameter. Here, super-refraction occurs when ASTD is positive. Sub-refractive conditions exist when DSTD is positive (RF) or ASTD is negative (IR). In oceanic environments the thermal stratification is usually near-neutral and the DSTD generally negative (since the dew point cannot be higher than the air temperature). Therefore, conditions over sea are frequently super-refractive at RF. Furthermore, sub-refraction cannot occur for both RF and IR and, therefore, at least one frequency must be in the super-refractive domain. This indicates the synergism and complementarity of IR and RF for long-range detection.

The SYLT92 campaign was organized in a coastal marine environment to simultaneously perform propagation experiments at radar and infra-red wavelengths and measure the detailed structure of the marine atmospheric surface layer (up to 30 m above the sea surface). The objective of SYLT92 was to study the behaviour of electromagnetic radiation over sea and to validate and improve current models predicting radar or infra-red propagation. The synergism between IR and radar detection systems can then be demonstrated via the models.

The SYLT92 experiment was a trilateral cooperation between institutes from Germany, Canada and The Netherlands. The experiment took place from May 18 until June 19 at the North Sea near the German island of Sylt. The campaign was coordinated by the TNO Physics and Electronics Laboratory, that also performed radar propagation measurements and was responsible for meteorological characterization of the atmospheric surface layer. Germany hosted the experiment. WTD-71 (Germany) made available the Hubinsel Barbara, a jack-up barge that was towed to an indicated position, and a service boat. FGAN-FHP (Germany) conducted radar measurements and had a meteorological station on one of the radar reflector poles. Wave information was made available from the tide gauge at Westerland. DREV (Canada) was responsible for the optical and IR propagation measurements. The SYLT92 experiment and the individual contributions, with emphasis on the efforts by the TNO Physics and Electronics Laboratory was extensively described by De Leeuw et al.[1]

An overview of the results from the RF propagation measurements was presented by Sittrop et al.[2], an initial analysis of the IR propagation measurements was presented by Dion and Beaulieu.[3]

In this contribution the results are presented of the analysis of meteorological data collected during the SYLT92 experiment and the validation of two models predicting the refractive structure of the atmosphere at radar and infra-red

Paper presented at the Sensor and Propagation Panel Symposium on "Propagation Assessment in Coastal Environments" held in Bremerhaven, Germany 19-22 September 1994.

wavelengths. The models predict temperature, humidity and refractivity profiles, which are compared to observed vertical variations. Discrepancies between model predictions and observations are ascribed to the influence of the nearby coast.

3. EXPERIMENTAL SET-UP.

The experimental set-up is briefly described, with emphasis on the meteorological measurements. The reader is referred to De Leeuw et al.[1] for a more detailed layout of the experiment.

The experiment was centred around the German jack-up barge 'Hubinsel' Barbara, placed in the North Sea, near the German coast. Temperature and humidity sensors were placed at different heights on the west side of the platform for profile measurements, up to about 30 m above sea level. Profiles were also measured along a mast with 4 sensors, placed at 4, 5, 7 and 9.5 m above mean low sea level. The height of the lowest sensor was such, that it was well away from the waves at high tide, allowing for waves up to 1.5 m.

Figure 1 shows the locations of the barge 'Barbara' and the mast.

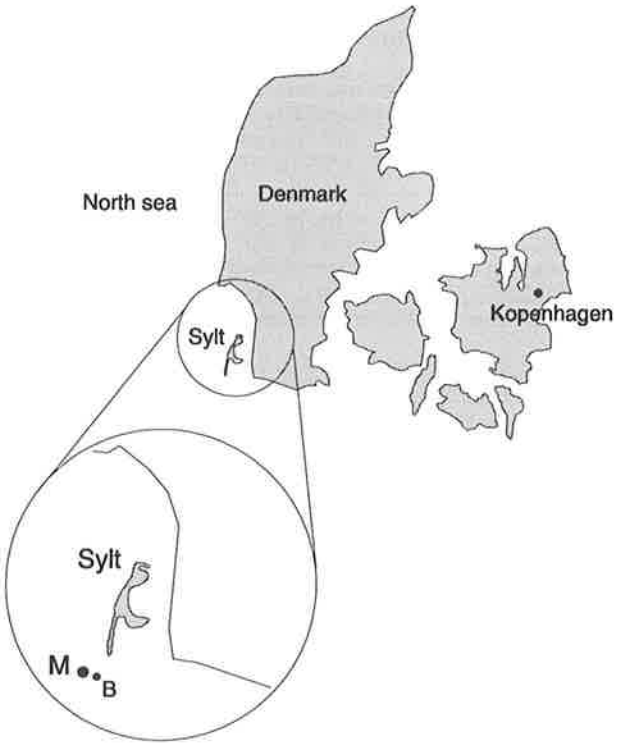

Figure 1. Locations of 'Hubinsel Barbara' and the mast.

The instruments on the mast were Rotronic Hygrometers, type YA-100 with teflon foam filter, placed in a Young shelter, shielding the sensors from sea spray and solar radiation. The instruments were placed in the prevailing wind direction, WNW to NW in June,[4] free from distortion effects from the Mast. A cup-anemometer was placed on top of the mast. Sea temperature was measured at 0.2 m below the sea surface, with a thermistor mounted on a float.

On Barbara, temperature and relative humidity were measured with Hygrophyl instruments, type G1463, mounted on the west side of the hull. In this way, the sensors would be exposed for the wind directions expected in the area. Wind speed and wind direction were measured with a cup anemometer and a wind vane, mounted in a mast on the helicopter deck, at a height of 35 m. Sea temperature was measured by two systems, each consisting of a thermistor on a float. Thus, possible contaminations from the platform could be detected.

In the mast on the helicopter deck of Barbara, also a turbulence package was mounted, consisting of a 3D sonic anemometer and an OPHIR IR hygrometer. Both these instruments measured at high frequency (25 and 20 Hz). Their results are not included in the present analysis.

Tidal data are taken from the tidal gauge at the Westerland tower, digitized from analog recordings. Correction curves have been applied to obtain the water height at the location of the mast.

4. DATA VALIDATION AND CALIBRATION.

4.1 Validation

During most of the experiment the wind came from easterly directions and most of the Barbara instrumentation was on the lee side of the platform structure. In that case the readings of these instruments were strongly affected by the platform and not representative for unperturbed open sea conditions. Therefore, they are not used in our analyses. The only instrument on Barbara that produced reliable data of both temperature and humidity was the Hygrophyl on the halfdeck (on average at 25 m above sea level). The Ophir instrument on the heli deck appeared to give unreliable humidity readings, although the temperature data seemed to be correct. Therefore the Ophir temperature is used where possible.

All of the sensors on the mast gave reliable results during the whole experiment, except for one occasion when sea spray apparently affected the lowest sensor.

4.2 Sensor comparison.

Temperature and humidity sensors were calibrated prior to the experiment and anemometers were compared. Nevertheless, the readings of different instruments, when calibrated, are known to be somewhat different, when a side-by-side comparison is made. However, for the evaluation of the gradients the differences between the instruments at the various levels and platforms are more important than the absolute values. Therefore, prior to installation of the instruments an intercomparison was made with all instruments mounted on the halfdeck, in the shadow of the helideck. Data were collected during a 24-hour period on May 19 and 20. These data comprise a balanced set, both at the low and at the high ends of the temperature and humidity ranges sufficient data are available to compute reliable correction curves. During the experiment, several additional comparison runs were made with the instruments placed side-by-side and whenever possible, the mast sensors were compared with a hand-held calibrated DV-2 temperature and humidity sensor. In

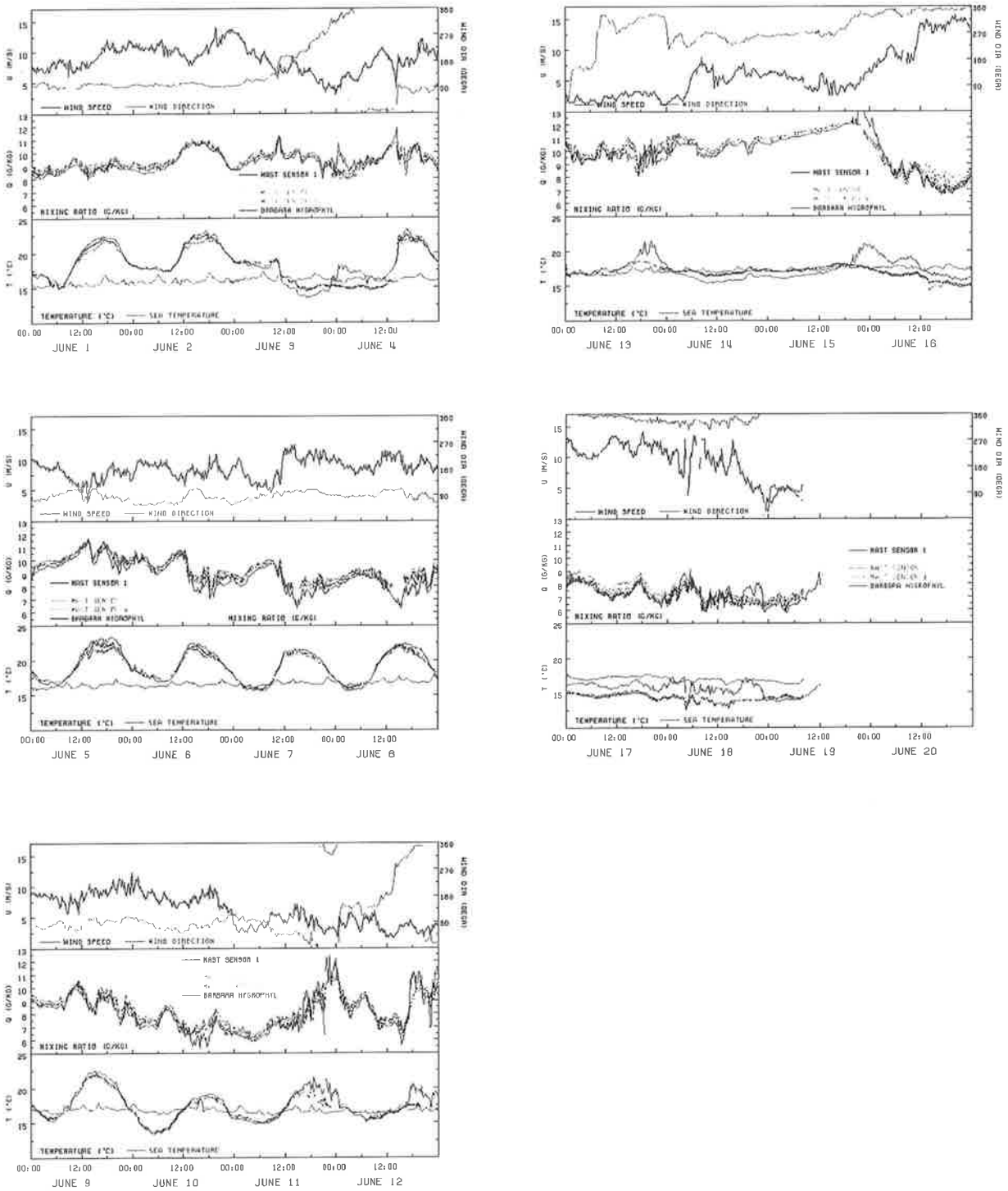

Figure 2. Overview of meteorological data measured during the SYLT92 experiment, June 1-19: upper panels show wind speed and direction, mixing ratios from the four mast sensors and the hygrophyl are shown in the middle panel, temperatures are shown at the bottom.

addition, the Barbara instruments were compared with an Assmann wet/dry bulb hygrometer, on a daily basis and sometimes several times per day.

The temperature sensor comparison data cover the temperature range 13-19 °C evenly; no data were obtained for higher temperatures. All Rotronic sensors consistently give temperatures about 0.5 to 0.8 °C lower than the three sea temperature sensors (thermistors). The latter were calibrated prior to the SYLT experiment with the thermistors in a climate chamber at TNO. For this reason, one of the sea temperature sensors of Barbara was chosen as reference.
The humidity calibration data cover a range of relative humidities from 55% to 90%. The mast hygrophyl sensors agree well; the only hygrophyl used on Barbara consistently yields lower humidities. No true calibration of the humidity sensors was made prior to the experiment, although all sensors were factory-calibrated. The sensor at the top of the mast is chosen as reference sensor, because its data compare well with the readings from hand-held instruments (Assman and DV-2).

For more details on the data comparison, the reader is referred to Neele and De Leeuw.[5]

4.3 Validated data.

With the data from the sensor intercomparison, described above, correction curves were computed. The (linear) corrections were applied to all data available. The validated temperature and mixing ratio data are shown in figure 2, together with wind direction and wind speed, for the period June 1 - June 19.

The first half of the measuring campaign can be characterized by a diurnal period of warming up during the afternoon and cooling during the night. This is associated with stable thermal conditions during periods of sunshine and, usually, unstable stratification during the night and morning. The wind was off-shore during this period (direction around 90°). During the stable periods, large ASTDs were observed, up to 7 °C between the lowest mast sensor and the sea surface. A stationary front between maritime and continental air masses passed the area on June 4, around 14:00h. It is marked by a abrupt increase in temperature and change in humidity; the wind direction changes from east through south to north and to east again.
During the second half of the campaign, roughly from June 12 onward, onshore winds dominated. Consequently, the ASTD was smaller, around zero and negative during the last few days. Note that whenever the wind was northerly, the sensor on Barbara's half deck gave unrealistically high temperatures and unrealistically low humidities.

The sea temperature varied with the periodic heating of sea water on the tidal flats near the shore: the peaks in the sea temperature record coincide with receding tide, when warm water from the tidal flats passed the sensors.

Figure 2 shows that the various meteorological parameters are not independent. In part this is due to coastal influences. For example, large, positive ASTD occurred only for off-shore winds; for onshore winds the ASTDs were small.

5. IR AND RF REFRACTIVITY.

Due to vertical and horizontal variations in humidity, temperature, pressure, etc., electromagnetic waves in the atmosphere are refracted. In super-refractive conditions, velocity increases with height and a ray leaving a source horizontally is bent towards the Earth's surface. Sub-refractive conditions exist when rays are bent upward (velocity decreasing with height). Trapping of rays in a layer near the surface occurs in the former case, when the rays are bent with a curvature greater than that of the Earth. In such conditions the range of radar or infra-red observations is not limited by the geometrical horizon and can be quite large (if not limited by extinction due to aerosols or molecular species). The height at which a ray is bent such that it travels parallel to the Earth's surface is called the duct height; this height is usually taken as the top of the trapping layer.

The refractivity profile can be calculated from the observed temperature and humidity profiles, because these parameters dominate the refractive structure, or refractivity profile (see below for definitions). The refractivity structure thus obtained may be used, for example, to predict maximum visibility range for radar or, by ray-tracing, to assess the use of IR and RF systems and their limitations due to atmospheric refraction and multipath effects.

5.1. Calculation of RF refractivity.

Since the variations in the index of refraction n are very small, the refractivity N has been introduced

$$N = (n-1) \cdot 10^6$$

Following Beaulieu,[6] the refractivity N for radar is calculated using the relation

$$N_{RF} = 77.6\ p / T + 3.734 \cdot 10^5\ V_p / T$$

where p is atmospheric pressure in mbar, T the air temperature in Kelvin and V_p the partial water vapour pressure in mbar. At the length scales typically involved in radar experiments, the curvature of the Earth's surface must be taken into account. The spherical geometry can be incorporated in two ways. One is by performing all calculations in a spherical geometry. The other is by transformation of the refractivity profile, using a flat-Earth representation, to exploit the simpler expressions of a flat geometry. For radar propagation close to the sea surface, a good approximation to the transformation to a flat-Earth representation is obtained by adding 0.157 times the height to the refractivity profile. Thus, the modified refractivity M is obtained. Using the previous expression for N, the modified refractivity is then given by

$$M_{RF} = 77.6\ p / T + 3.7345 \cdot 10^5\ V_p / T + 0.157\ z$$

where z is the height (in m) above the sea surface.

5.2. Calculation of IR refractivity.

The IR refractivity is found using the formula given by Edlén :[7]

$$M_{IR} = \left[a_0 + \frac{a_1}{(1 - (\nu/b_1))} + \frac{a_2}{(1 - (\nu/b_2))} \right] \cdot \frac{p\,(T_0 + 15.0)}{p_0\,T} - \frac{p_w}{p_0} \left[c_0 - (\nu/c_1) \right]$$

where p is atmospheric pressure (mbar), T the air temperature (Kelvin), p_w the partial water vapour pressure (mbar). The wavelength dependence is incorporated in the formula through the wavenumber v:

$$\nu = 1 \cdot 10^4 / l$$

where l is the wavelength in μm. The constants in the formula of Edlén are

$a_0 = 83.42$ $\quad b_1 = 1.140 \cdot 10^5$ $\quad c_0 = 43.49$
$a_1 = 183.08$ $\quad b_2 = 6.240 \cdot 10^4$ $\quad c_1 = 1.7 \cdot 10^4$
$a_2 = 4.11$

$T_0 = 273.15\ K$
$p_0 = 1013.25\ mbar$

We calculated the refractivity for IR wavelengths of 1.06 μm (Nd/YAG laser) and 10.59 μm (CO_2 laser and thermal IR systems), using the meteorological data discussed in the previous section.

6. MODEL VALIDATION.

With the present data set, models describing the structure of the atmospheric surface layer over water can be evaluated for a coastal area. The behaviour of temperature and humidity as a function of height above the sea level predicted by these models is generally of the logarithmic type. This is valid in near-neutral conditions, with no coastal influences. The site chosen in this experiment is close to the German coast; the effect of nearby land is expected for easterly winds.

The following sections deal with the validation of two models, LKB[8] and EVAP.[9] Discrepancies between observations and model are related to specific weather parameters.

6.1 The models

6.1.1 LKB model

The LKB model[8] is based on a bulk parameterization of the fluxes of heat, moisture and momentum between atmosphere and ocean. An interfacial sublayer, a thin layer above the sea surface where molecular diffusion processes are important, is incorporated in the model. It is applicable in approximately stationary and horizontally homogeneous conditions, over an open fetch of water and with moderate wind speeds. The model incorporates the effect of wind-generated waves on the local roughness (effects of swell are not included in the model). The authors expect that at high winds the model breaks down, as breaking waves disturb the interfacial sublayer and sea spray affects the temperature and humidity in the surface layer.

The model calculates the profiles of temperature and humidity from the measured values at a single height. With these profiles, the refractive structure (see previous section) can be calculated; the duct height is then simply the minimum in the modified refractivity profile.

In this study the implementation of the LKB model by Liu & Blanc[10] is used, extended with a routine to find $M(z)$.

6.1.2 EVAP model

The EVAP model[9] is based on the theory developed by Jeske.[11] This model directly estimates the duct height from the bulk meteorological measurements. The method approximates the gradients of temperature and humidity by their vertical differences (sensor height - surface). This is justified when the gradients are small (near neutral conditions), but may lead to under- or overestimating of the duct height for highly (un)stable stratification. For such conditions, no generally accepted models exist.[11] The theory does not incorporate an interfacial sublayer and assumes a constant roughness length z_0. Geernaert[12] showed that z_0 depends on wave state (and wind stress).

The theory on which the EVAP model is based, does not incorporate a molecular diffusion layer, like the LKB model. Starting from the flux-gradient relations from turbulence theory for temperature and humidity, the M-profile is developed. Jeske[11] and Paulus[9] do not present explicit formulae for the temperature and humidity profiles. Their formulation differs from that of Liu et al. (1979) in the approximation of the vertical gradients by a different formula. The stability function Φ is also formulated in a different way.

The original EVAP model[9] assumes that the measurements are made at a height of 6.5 m above mean sea level (AMSL). For the present study, the model has been modified to accept any measurement height. For the present situation, the difference is small, as the height of the highest mast sensor (used as reference) is around 10 meters. Nevertheless, the modified model yields results that are in better agreement with observations than the original EVAP model.

6.2 Validation of temperature and humidity profiles

6.2.1 Temperature

The readings from the highest sensor on the mast, together with the wind speed and the sea temperature data, are used in the LKB and EVAP models to compute the profiles of temperature and relative humidity. A comparison between observed and computed temperature profiles is shown in Figure 3. The time period presented in the figure is June 3 and 4. Temperature profiles are plotted every hour; the temperature axis is horizontal, increasing to the right. The logarithm of height is plotted on the vertical axis. Throughout June 3 and most of June 4 almost purely logarithmic profiles are observed. The sudden change in the profiles around 14:00h on June 4 is due to the passage of the stationary front. At that time, the conditions changed from unstable to stable, with ASTD > 5°C. The LKB model predicts a temperature gradient that is too high (solid lines), where the EVAP profiles compare better with observations. For near-neutral conditions, as observed in the second half of the measuring period, the temperature profiles are almost purely logarithmic and the two models agree very well (not shown). The largest discrepancies appear for large, positive ASTD. Jeske[11] (1973) already noted that in these cases the assumptions in the EVAP model break down.

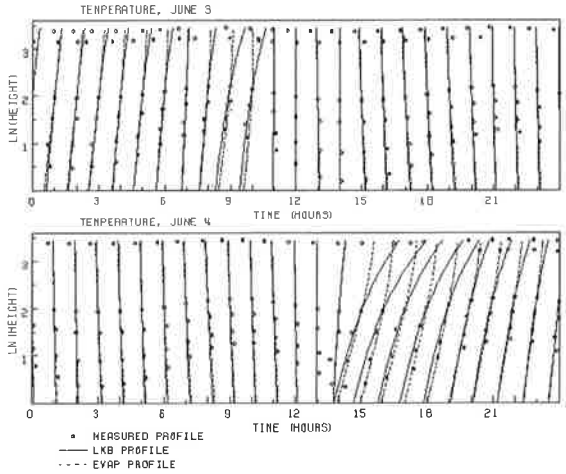

Figure 3. Comparison of temperature profiles computed with the LKB and EVAP models with experimental data. See text for explanation.

The difference between the modelled values for temperature or humidity and the respective observed values at the lowest sensor is used as a measure of the misfit between model and observations. Since the lowest sensor is furthest away from the reference sensor, deviations of the computed profile from the observed one show up clearest at this sensor. The data (i.e., differences between model and observation) are presented in scatter plots, organised as a function of wind speed, wind direction, tide or ASTD. Figure 4 shows an example of a scatter plot, obtained for the LKB model. The data are plotted as a function of wind speed, in different panels corresponding to increasing ASTD. Error bars are obtained by binning the data (in the case of Figure 6 in bins 1 m/s wide) and computing the mean and standard deviation. For this a robust technique of iterative residual down-weighting[13] is used. This method iteratively downweights all data that lie further than a specified number of standard deviations from the mean; in this case 1.5 standard deviations is used.

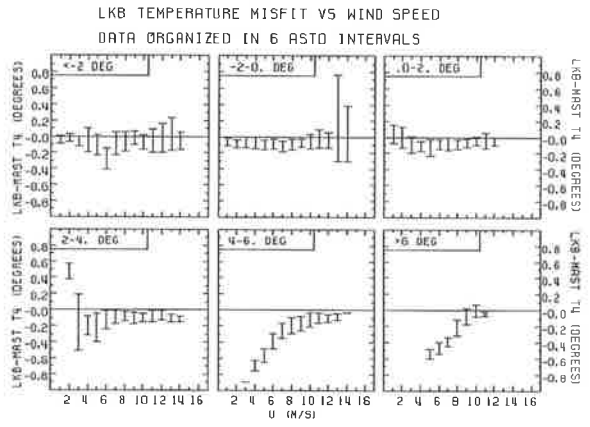

Figure 4. Scatter plot of temperature misfit against wind speed. Temperature misfit is defined as LKB-computed minus temperature observed at the position of the lowest sensor on the mast. Input for the LKB model were the observations from the highest sensor on the mast. Data are arranged in intervals of increasing ASTD.

In this way, outliers in the data set have a minimized influence on the mean temperature or humidity. The uncertainty in the individual measurements is 0.2°C, which compares well with the error bars in Figure 4. As noted before, large positive air-sea temperature differences occur in off-shore winds. In these cases a clear trend is visible of increasing model misfit as the wind speed is lower (cf. the data in the panels where ASTD > 4°C).

Figures 5 and 6 are similar to Figure 4, but now the data for increasing height AMSL of the lowest sensor are plotted as a function of wind speed. The height variations are caused by tidal effects. Data plotted are for off-shore winds only (wind directions between 60° and 120°), and ASTD greater than 3°C. It is clear that the trend increases with decreasing distance from the sea surface. At heights above 3.5 m the model compares favorably with experimental data. The data in Figure 5 are for the LKB model, those in Figure 6 are for the EVAP model. The EVAP model predicts temperatures near the sea surface that are too high. This is probably due to the absence of a surface boundary layer in the EVAP model. As the LKB model is the more complete of the two models tested here, it seems that the LKB model is more likely to represent the behaviour of open ocean atmosphere.

Figures 4 and 5 strongly suggest the existence of an additional boundary layer, formed for off-shore winds, when relatively warm air masses from land move over a cold sea surface. In this new boundary layer the temperature is higher than expected (temperature difference negative) from the model predictions. The thickness of this boundary layer would be about 3 m for low wind speeds, estimated from the maximum height above the sea at which the effect is visible in figure 5. At high winds the boundary layer disappears completely. Such an inverse relation of boundary layer thickness with flow speed is expected.[14]

Note in the figures that the LKB model tends to underestimate the temperature at the position of the lowest sensor. This is apparent from a bias toward negative temperature misfits in figure 4. A problem with the present data set is the measurement of the sea temperature. The sea temperature sensor measured the temperature at about 0.2 m below the sea surface. This temperature may deviate from the skin temperature by up to 0.5 °C (see, e.g., Roll[15] and Soloviev[16]). However, the LKB and EVAP models require the skin temperature as input. The effect of using the sub-surface sea temperature is difficult to assess. Roll[17] noted the existence of a 'cold film' on the sea surface, due to cooling by evaporation. In temperate environments the sea nearly always acts as a source of water vapour and this 'cold film' would be expected to be present. The magnitude of the temperature drop in this film is not quite clear. Liu et al.[8] note that the error introduced by using the sub-surface temperature would be largest for ASTD near zero.
In general, the largest scatter of model temperature minus observed temperature occurs for stable conditions, which arise almost exclusively for off-shore winds. This shows that coastal effects may reduce the applicability of the models tested here.

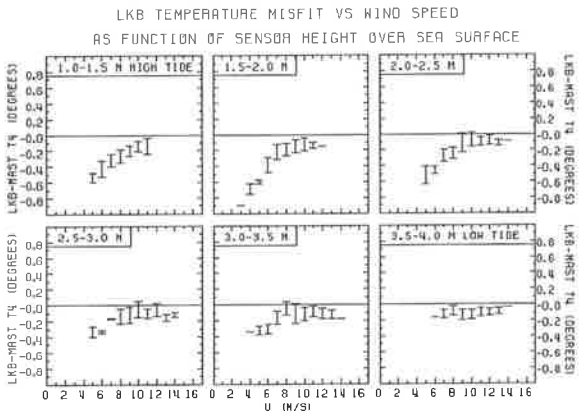

Figure 5. As figure 4, now only for wind directions between 60° and 120° (off-shore winds). Parameter is the height AMSL. The misfits show a trend of decreasing misfits with increasing wind speed. This trend is largest when lowest sensor on the mast is close to the sea surface (high tide) and disappears when sensor is more than about 3 m over the sea surface.

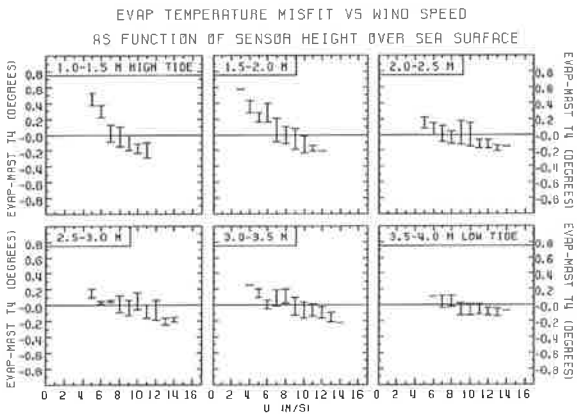

Figure 6. As figure 5, now for the EVAP model. The misfits for this model show a trend that is opposite to that in figure 5. The lack of an interfacial sublayer in this model may be the cause for this.

6.2.2 Humidity

The shortcomings of the EVAP model are most obvious in the humidity profiles (mixing ratio). An example is shown in Figure 7, for June 13 and 14. Both experimental data and profiles computed from the two models used in this study are shown. The EVAP model predicts dramatical increase or decrease in the humidities with height. The weather conditions on June 13 include ASTD near 0°C and low wind speeds (below 2 m/s). For such low wind speeds the flow is smooth, rather than rough. The smooth flow results in very small L' (Monin-Obukhov lengths corrected for stability, as used in the EVAP model) and hence large values of z/L'. The stability function Φ used in the EVAP model is valid for small values of its argument z/L', yet the small value of L' leads to unreliable results. The LKB model uses a different formulation of the Monin-Obukhov length, which does not approach zero for low winds. Therefore, this model predicts humidity profiles that are much closer to the observed profiles.

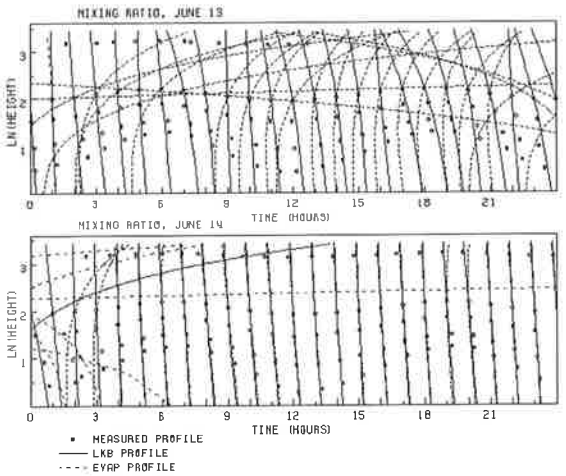

Figure 7. As figure 3, now for mixing ratio in the two-day period June 13 and June 14. The predictions from the EVAP model are unreliable, due to low wind speeds.

Brutsaert[18] (1992) presents alternative approximations for the stability function Φ, that are valid for a much larger range of its argument, but these have not been tested here. It should also be noted that the formulations used for Φ are based on data collected over land. Schacher et al.[19] showed that over water different relations apply. For unstable conditions over water, McBean and Elliot[20] derived a relation yielding better results than a relation valid for over-land experiments; no such relations are available for unstable or neutral conditions over water. The results of Davidson and Boyle[21] also suggest that such relations are needed for over-water experiments.

6.3 Refractive structure of the atmosphere

Using the theory presented in section 5 and the profiles of temperature and humidity, the refractive structure of the surface layer can be calculated. It should be kept in mind that in this experiment the temperature and humidity profiles have been measured locally. Spatial variation of T and Q do occur in this coastal area with off-shore winds but have not been measured. These spatial variations may have a stronger effect on the propagation of electromagnetic radiation than vertical gradients, especially in the present coastal environment. For onshore winds, such gradients are expected to be relatively small, as the air masses have been mixed thoroughly.

6.3.1 Radar refractivity

Figure 8 shows some results for the radar refractivity profiles, for June 1 and June 13, respectively. Profiles are shown every hour; horizontal axis is height, vertical is modified refractivity M. During the first part of the experiment, the two models give similar results. The LKB model predicts profiles that increase more rapidly with height than EVAP; this agrees with the data from the Hygrometer on Barbara's half deck. The weather conditions on June 13, as discussed above, are such that the EVAP model predicts non-ducting conditions during most of the day. This is in clear disagreement with the data. The LKB model yields profiles that are in better agreement with the experimental data.

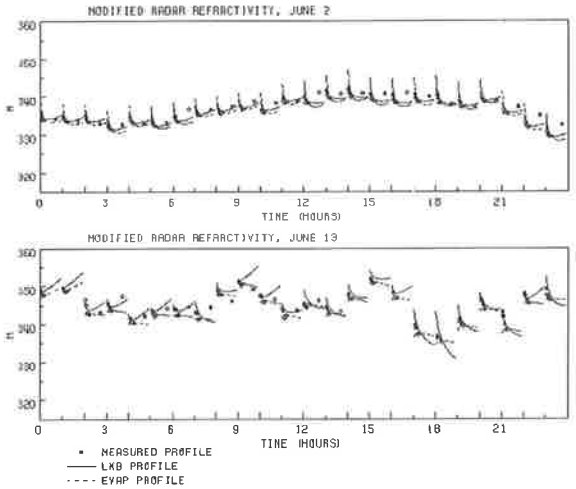

Figure 8. As figure 3, now for modified radar refractivity, for June 2 and June 13. Whereas both the LKB and EVAP model give good results during June 2, the low wind speeds on June 13 cause a break-down of the EVAP model.

The data in Figure 8 are an ilustration of the common occurrence of super-refractive conditions for radar frequencies. Both data and model predictions indicate that during the greater part of the experiment the conditions were such that radar waves are trapped near the surface. Such conditions are favourable for radar detection over long ranges.

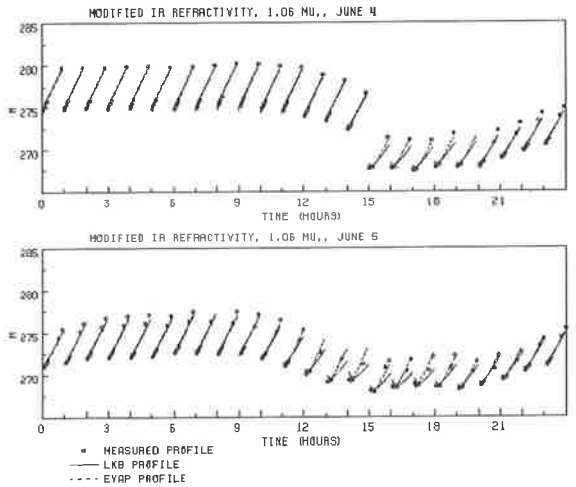

Figure 9. As figure 3, now for modified refractivity at the infra-red wavelength of 1.06 μm. Period displayed is June 4 and 5. Sub-refractive conditions prevail, indicated by monotonously increasing *M*. During the afternoon on both days, the infra-red refractivity enters the sub-refractive domain.

6.3.2 Infra-red refractivity

The conditions for infra-red wavelengths are the opposite to those of radar. Some refractivity profiles are shown in figure 9, for a wavelength of 1.06 μm. The results for a wavelength of 10.59 μm are similar. The period covered is June 4-5. It is evident from Figure 9 that most of the time sub-refractive conditions prevail, indicated by the monotonously increasing $M(z)$. Super-refractive conditions exist only during the afternoon, when the ASTD is positive.

6.4 Duct heights

As described above, the height at which the modified refractivity profile has zero gradient is defined as the duct height. The observed duct height is found by fitting a linear+logarithmic function to the observed refractivity profile. The log-linear profile shape is suggested by the LKB and EVAP models. However, this fitting procedure amounts to introducing *a priori* knowledge about the shape of the refractivity function and leads to (unknown) errors if the true shape of this profile cannot be adequately described by a linear+logarithmic function. Fitting the observed profile with a different function (e.g., a second order polynomial) does not solve this problem.

For the determination of duct heights, the half-deck sensor on Barbara is used as well as the mast sensors. This is because it is essential for a reliable duct height estimate to have a measurement at some height above the mast. However, whenever the Barbara sensor gave unreliable

6.4.1 Radar (RF) ducts

Figure 10 shows the observed RF duct heights as a function of time, at 20-minute intervals, for the whole experiment. Also shown are the duct heights from the LKB and EVAP models. A clear diurnal pattern caused by heating and cooling is seen from June 5 to June 10. During the night, unstable conditions prevail and ducts are observed below 10 m height (evaporation duct). In the afternoon, when the atmosphere is warmed up by solar irradiation, stable conditions exist and no duct below the Barbara sensor is observed (leaving open the possibility of an elevated duct). The data show that for radar frequencies the conditions are predominantly super-refractive. During periods of stable conditions (warm air over cold sea), the models fail to produce reliable duct heights. For unstable conditions good performance is obtained. This result is supported by the data obtained from radar measurements.[1] During stable conditions radar cross sections show significantly larger scatter than when conditions are unstable. The LKB model seems to predict duct heights that are closer to the observed heights than the EVAP model, which is biased to too high ducts.

This result is shown in figure 11, which is a scatter plot of LKB and EVAP vs. observed duct heights. The high ducts predicted by LKB (above 20 m) all correspond to stable conditions.

6.4.2 Infra-red ducts

It has been noted that IR and RF are complementary in the sense that usually at least one of the two is in the super-refractive domain.[1,8] This allows one to be able to look beyond the geometrical horizon when sensor systems are available for both the IR and RF bands.

Figure 12 shows the duct heights at infra-red wavelength of 1.06 μm for June 5-8. The conditions are predominantly sub-refractive, the energy being bent away from the Earth's surface. During the first 8 days of the experiment, ducting is present during the afternoon. Similar results are obtained for a wavelength of 10.6 μm.

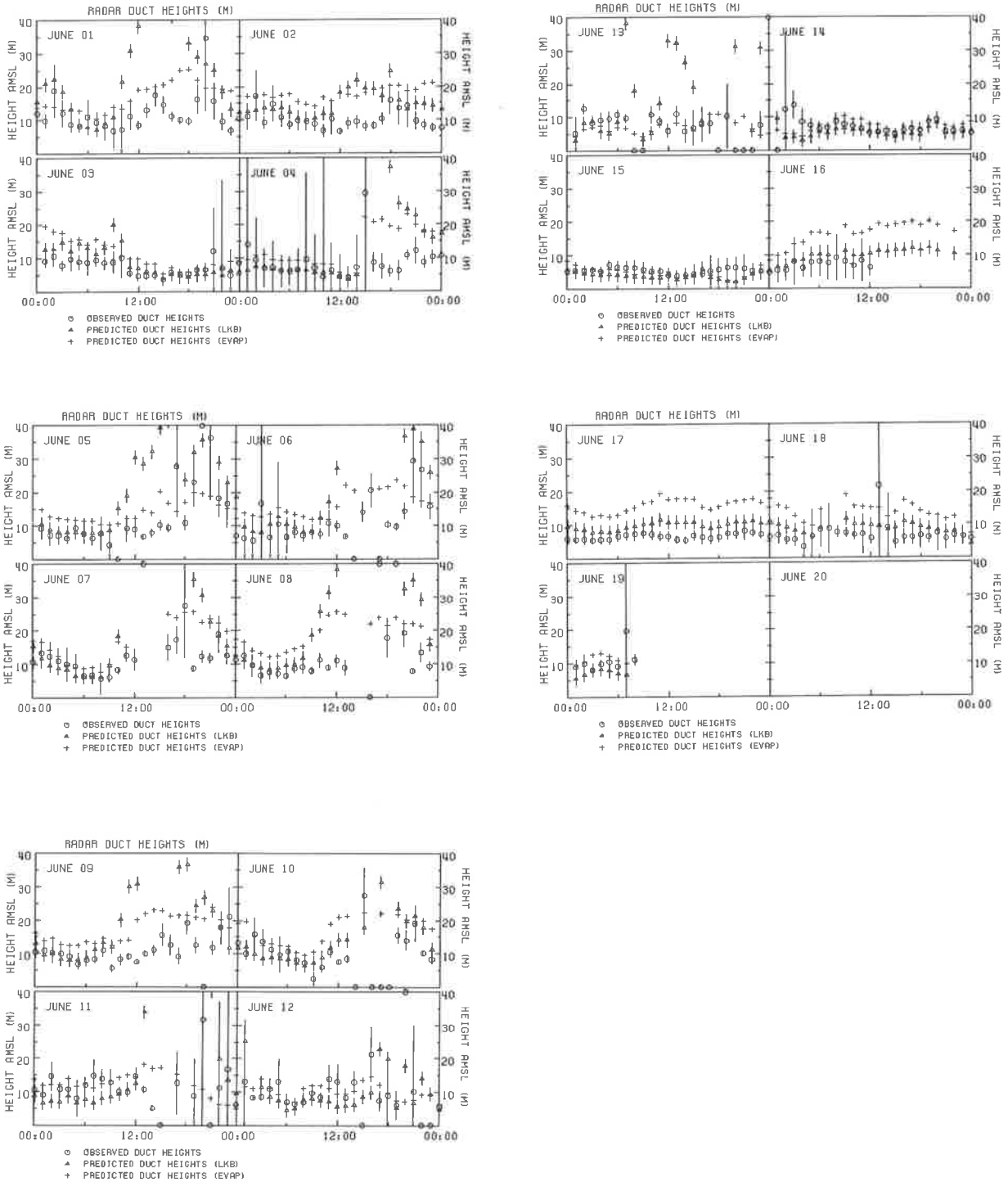

Figure 10. Variation of duct height at radar frequencies with time. Circles: observed duct height, triangles: LKB-predicted duct height and crosses: EVAP-predicted duct height.

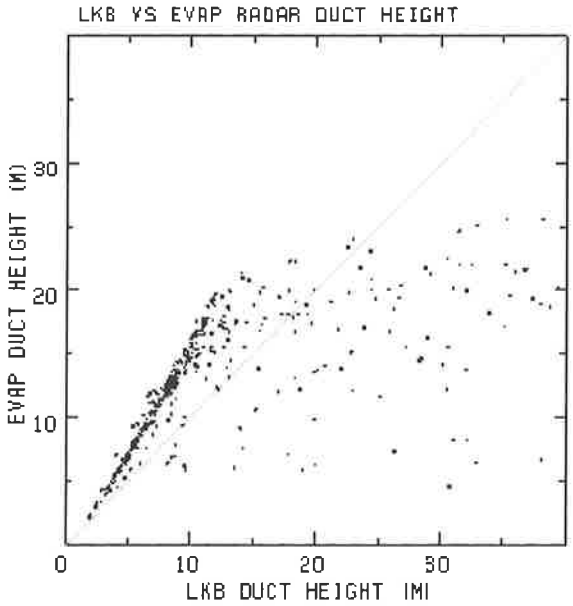

Figure 11. Scatter plot of duct heights predicted by the EVAP model vs. duct heights predicted by LKB model. The EVAP model is biased to high ducts, compared to the LKB model. All points where LKB predicts a duct height much larger than the EVAP model are associated with thermally stable conditions and offshore winds.

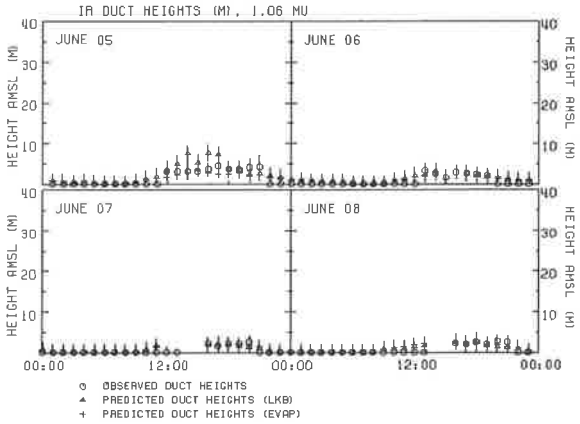

Figure 12. As figure 10, now for infra-red wavelength 1.06 μm, and the four-day period June 5 - 8.

A few times during the experiment a mirage effect has been observed visually. At these times the infra-red refractivity profiles show no sign of complexity or super-refraction. This is probably due to horizontal inhomogeneity of the atmosphere (the line of sight being in the direction of land) and the instruments being placed outside the complex zone.

Figures 10 and 12 are an indication of the complementarity of radar and infra-red with respect to super-refraction. Beaulieu[6] noted that always one or both of radar or infra-red is in the super-refractive domain. During the afternoon, when at radar frequencies no duct is detected within the height range of the sensors, the propagation conditions at infra-red wavelengths are super-refractive. This observation is a clear illustration of the value of combining RF and IR for long-range observation.

7. CONCLUSIONS.

The results presented in this report lead to the following conclusions.

The LKB model predicts reliable temperature and humidity profiles for both stable and unstable conditions, although for very stable stratifications the predicted gradients are too large. Duct heights produced by the model are in good agreement with observations for unstable conditions.

The EVAP model is based on more assumptions about the structure of the atmospheric surface layer and simplifications in the theory than the LKB model. This results in duct heights that are biased to values that are too high as compared with observations. This is not due to the fixed measuring height, that was part of the original EVAP model; the model has been modified to accept the actual measuring height. The EVAP model produces unrealistic profiles of temperature and humidity for warm air moving over a cold sea surface, especially during light winds. This combination leads to unreliable duct heights, the cause for which must be sought in a small value of the Monin-Obukhov length used in the model. This results in a breakdown of the stability function Φ. This presents less of a problem in the LKB model, which uses a different formulation of the Monin-Obukhov length. For unstable conditions the EVAP model produces results that are in good agreement with observations, although it is biased to too high ducts.

In general, for unstable to neutral conditions, which in this experiment occur mostly for air masses with an oceanic origin, the data show that current models reliably predict the profiles of temperature and humidity in the atmospheric surface layer over the ocean, given a measurement at a single height. The fact that for stable conditions both models fail to reproduce the observations can be attributed to coastal influences. Stable conditions almost invariably occurred during the afternoon, when the wind was off-shore. The mast was located about 15 km off-shore, which is much closer than the estimated 60 km over which coastal influence has been shown to be present.[22] The high ASTD (up to 7°C between the lowest mast sensor and the sea surface) observed for off-shore winds indicate that these air masses have been warmed up over land and travelled a relatively short distance over the sea.

Thus, the data collected during SYLT92 strongly suggest that, for prediction of the behaviour of electro-optical and radar systems in coastal environments, current models of the atmospheric surface layer over the ocean need to be extended to include effects of nearby land. The possibly large temperature differences between the land and sea surfaces may give rise to a turbulence, stronger than expected if an oceanic origin is assumed for the air masses. Although the present data do not explicitly show this, strong horizontal gradients are expected in coastal areas for off-shore winds. Such gradients must be accounted for in any model predicting infra-red or radar propagation close to the sea surface in coastal regions.

ACKNOWLEDGEMENTS

Our participation in the Sylt92 experiments were supported by the Dutch Ministry of Defence, assignments A92KM609 and A92KM638. Hubinsel Barbara was made available through BWB-FFV-4, Koblenz and WTD-71. The support and advice of many colleagues at TNO Physics and Electronics Laboratory and elsewhere is gratefully acknowledged.

REFERENCES.

1. De Leeuw, G., Sittrop, H. and H.J.M. Heemskerk, First impressions and some qualitative results from the SYLT92 experiment, *TNO report 92-A363*, 1992.

2. Sittrop, H., H. Gravesteijn and H.J.M. Heemskerk. The influence of the evaporation duct on the angle of arrival and amplitude of the backscattered signal from targets low above the sea. in: Atmospheric propagation effects through natural and man-made obscurants for visible to mm-wave radiation. AGARD CP 542, paper 4 (13 pp.). 1993.

3. Dion, D. and A.J. Beaulieu. Sylt'92 campaign: the complementarity of radar and eo sensors. Defence Research Establishment Valcartier, Quebec, Canada, 1993.

4. Korevaar, C.G., *North Sea Climate, based on observations from ships and light vessels*, Kluwer, Dordrecht, The Netherlands, 1990.

5. F.P. Neele and G. de Leeuw. Temperature and humidity profiles from SYLT92: validation of RF and IR propagation models. TNO Physics and Electronics Laboratory, Report, 1994, in print.

6. Beaulieu, A.J., Atmospheric refraction model, Canada National Defence Research Establishment Valcartier, Québec, Rep. 4661/92, 1992.

7. Edlén, B., The dispersion of standard air, *J. Opt. Soc. Am.*, 43, 339-343, 1953.

8. Liu, W.T., Katsaros, K.B. and J.A. Businger, Bulk parameterization of air-sea exchanges of heat and water vapour including the molecular constraints at the interface, *J. Atmos. Sc.*, 36, 1722-1735, 1979.

9. Paulus, R.A., Specification for environmental measurements to assess radar sensors, NOSC TD 1685, San Diego, 1989.

10. Liu, W.T. and T.V. Blanc, The Liu, Katsaros and Businger (1979) bulk atmospheric flux computational iteration program in Fortran and Basic, NRL Memorandum Report 5291, 1984.

11. Jeske, H., State and limits of prediction methods of radar wave propagation conditions over sea, in *Modern Topics in microwave propagation and air-sea interaction*, A. Zancla (editor), p. 130-148, Reidel, 1973.

12. Geernaert, G. Bulk parameterizations for the wind stress and heat fluxes. In: G.L. Geernaert and W.J. Plant (Eds.): Surface waves and fluxes, Volume I - Current theory. Kluwer, Dordrecht, 1990.

13. Huber, P.J. *Robust Statistics*, John Wiley, New York, 1981.

14. Montgomery, R.B., Observations of vertical humidity distribution above the ocean surface and their relation to evaporation, *Papers in Phys. Oceanog. and Met.* v. 7, no. 4, 30 pp., 1940.

15. Roll, H.U., Über die vertikale Temperaturverteilung in der wassernahen Luftschicht, *Ann. Meteorol.*, 7, 4, 1948.

16. Soloviev, A.V., Coherent structures at the ocean surface in convectively unstable conditions, *Nature*, 346, 157-160, 1990.

17. Roll. H.U., Physics of the marine atmosphere, Academic Press, New York, 1965.

18. Brutsaert, W., Stability correction functions for the mean wind speed and temperature in the unstable surface layer, *Geophys. Res. Lett.*, 19, 469-472, 1992.

19. Schacher, G.E., Davidson, K.L., Houlihan, T. and C.W. Fairall, Measurements of the rate of dissipation of turbulent kinetic energy over the ocean, *Boundary Layer Meteorol.*, 20, 321-330, 1981.

20. McBean, G.A. and J.A. Elliot, The vertical transports of kinetic energy by turbulence and pressure in the boundary layer, *J. Atmos. Sci.*, 32, 753-766, 1975.

21. Davidson, K.L., and P.J. Boyle. Overwater results on the dimensionless TKE dissipation rate. Proc. Ninth Symp. on Turbulence and Diffusion, Roskilde, Denmark, April 30-May 5 1990, 51-53.

22. EPRF (Environmental Prediction Research Facility), Coastal sea-air interactions and the extent of coastal influence, Techn. Note, 72-2, Naval Postgraduate School, Oceanographic Dept., Monterey, 1972.

DISCUSSION

J.H. RICHTER (Comment)
The importance of the horizontal variability of surface layer properties (such as the effect of air-sea temperature differences on refractivity) is generally different for infrared as opposed to microwave operational applications. In the microwave case, usually ranges of tens to hundreds of kilometers are of interest while infrared systems are mostly used for ranges that are an order of magnitude smaller. This may result in different sampling and prediction requirements for infrared and microwave applications.

R. PAULUS
The EVAP model operates in terms of potential refractivity. How is mixing ratio extracted from that?

AUTHOR'S REPLY
The EVAP model is based on Jeske (1973) and we have used his formulation for surface layer profiles in our calculations. The equation for direct calculation of refractivity profiles in the EVAP model is based on the explicit gradients of temperature and humidity.

D. DION
Even though discrepancies are observed between measured and predicted values for the lowest probes, don't you think that the real question is which profiles lead to better predictions of propagation effects? What do the results say?

AUTHOR'S REPLY
Of course, the real question is which profiles lead to better predictions of propagation effects. However, models are based on theoretical formulations that have to be tested with experimental data. Our aim of this analysis was to study the effect of waves and thermal stratification on model formulations. The results have been presented here. From the same experiment, also RF and IR-propagation measurements are available. The analysis of the RF propagation measurements has shown some unexpected effects which could be qualitatively explained with the meteorological observations. The quantitative test of the propagation models with these RF propagation data is outside the scope of the present paper.

S. BURK
You encountered trouble with low winds speeds in the Liu, Katsaros, Businger formulation. Have you tested artificially constraining the wind speed to be no smaller than some value, say 2 m/s, and see what results from such calculations?

AUTHOR'S REPLY
We have not tested with artificial constraints. The discrepancy between LKB model predictions and observations are only found for very large values of ASTD and low wind speeds, i.e., a very stable atmosphere. If only the wind speed is low, but the thermal stratification is unstable or neutral, the LKB model gives much better predictions. Hence, we infer that the observed discrepancies cannot be attributed to a general failure of LKB in low wind speed conditions, rather we ascribe the discrepancies to the occurrence of a non-equilibrium situation of warm air flowing out over a cold sea surface. This gives rise to an internal boundary layer for which models are presently not available.

AGARD-CP-567

AGARD-CP-567

AGARD

ADVISORY GROUP FOR AEROSPACE RESEARCH & DEVELOPMENT
7 RUE ANCELLE, 92200 NEUILLY-SUR-SEINE, FRANCE

AGARD CONFERENCE PROCEEDINGS 567

Propagation Assessment in Coastal Environments

(l'Évaluation de la propagation en régions côtières)

Papers presented at the Sensor and Propagation Panel Symposium, held in Bremerhaven, Germany 19-22 September 1994.

NORTH ATLANTIC TREATY ORGANIZATION

Published February 1995

Distribution and Availability on Back Cover